Catal Lett (2008) 126:325–332
DOI 10.1007/s10562-008-9624-0

A Comparative Study of Partial Oxidation of Methanol over Zinc Oxide Supported Metallic Catalysts

Wang Jianxin · Luo Laitao

Received: 12 July 2008 / Accepted: 20 August 2008 / Published online: 18 September 2008

Abstract Au/ZnO, Pd/ZnO and Au–Pd/ZnO catalysts were prepared by PVP-stabilized reduction method by C_2H_5OH. The catalysts have been used successfully for hydrogen production by partial oxidation of methanol (POM). The influence of Au, Pd and Au–Pd on the performance of supported catalysts for POM has been investigated. The prepared samples were characterized by ICP, XRD, BET, TPR and TPD. The results show that the Au–Pd/ZnO catalyst are more active and exhibit higher hydrogen selectively compared to the Pd/ZnO and Au/ZnO catalyst, the methanol conversion of 99.5% and hydrogen selectivity of 65.6% were obtained at 573 K. The enhanced activity and stability of the bimetallic Au–Pd/ZnO catalyst has been explained in terms of the higher dispersion and basic density, smaller particles of gold and synergetic effect between gold and palladium.

Keywords Au–Pd catalyst · ZnO support · Partial oxidation of methanol · Hydrogen generation

1 Introduction

Fuel cell technology is promising for efficient conversion of chemical energy into electrical energy with negligible emission of pollutant [1]. There are many type of fuel cell under development. Among them, the proton exchange membranes fuel cell (PEMFC) is the most promising fuel cell and may be applied to mobile cars, cell phones and notebook computers. However, the application is hindered by technical difficulties in storage, transportation and distribution of hydrogen. The difficulties may be avoided by an on-board production of hydrogen from liquid fuels. Methanol is a promising fuel candidate because of its easy handling, high H/C ratio, and low price [2]. Hydrogen may be produced directly from methanol according to a number of different processes such as methanol decomposition (MD) [3], steam reforming (SRM) [4, 5], oxidative steam reforming (OSRM) [6, 7] and partial oxidation (POM) [8–11].

$$\text{DM} \quad CH_3OH \rightarrow 2H_2 + CO \quad \Delta H^{\circ}_{298\,K} = 90.1\,\text{kJ/mol} \tag{1}$$

$$\text{SRM} \quad CH_3OH + H_2O \rightarrow 3H_2 + CO_2 \quad \Delta H^{\circ}_{298\,K} = 49.0\,\text{kJ/mol} \tag{2}$$

$$\text{POM} \quad CH_3OH + 1/2O_2 \rightarrow 2H_2 + CO_2 \quad \Delta H^{\circ}_{298\,K} = -192.2\,\text{kJ/mol} \tag{3}$$

$$\text{OSRM} \quad CH_3OH + 1/2H_2O + 1/4H_2 \rightarrow 5/2H_2 + CO_2 \quad \Delta H^{\circ}_{298\,K} = -12\,\text{kJ/mol} \tag{4}$$

Partial oxidation of methanol (POM, Eq. 3) in the absence of steam offers several advantages over steam reforming, as the reaction is exothermic, uses air or oxygen as oxidant instead of steam and so steam generation unit is not required. Therefore, POM has been suggested as a suitable route for hydrogen extraction from methanol.

The POM reaction had been studied over copper [12] and palladium based [8, 9] catalysts. Unfortunately, these catalysts produce considerable amount of carbon monoxide as a by-product. CO is a poison to fuel cell anodes. If the carbon monoxide level exceeds a few ppm, the precious metal-based anode electrocatalyst of the fuel cell is

W. Jianxin · L. Laitao (✉)
Institute of Applied Chemistry, Nanchang University, Nanchang 330031, Jiangxi, China
e-mail: luolaitao@163.com

deactivated. Recently, Chang et al. [13, 14] have produced a fruitful result on the production of hydrogen by POM using supported gold catalysts. They found that the gold based catalysts exhibited high methanol conversion and hydrogen selectivity with little content of CO. It is reported that the supported Au catalysts exhibited high activity for CO oxidation in the low-temperature [15]. However, the supported Au catalysts are easy to be sintered at high temperature, the addition of the second component may induce significant changes in both activity and stability for catalytic reactions [16, 17]. Further development of new efficient catalyst systems that exhibit an improved long-term stability and selectivity towards hydrogen production are highly desired. In the present work, the catalytic activity of Au–Pd/ZnO catalyst was studied for the formation of hydrogen by POM. The reason for choosing Au–Pd/ZnO catalyst is, supported palladium based catalyst is reported to be active for POM to produce hydrogen [8, 9]. Since supported gold catalysts are active for POM to produce hydrogen, a combination of gold and palladium metals was used in the present study.

The objective of the present investigation is to compare the catalytic activity and stability of Au/ZnO, Pd/ZnO and Au–Pd/ZnO catalysts prepared by PVP-stabilized reduction method by C_2H_5OH for the formation of hydrogen by POM. In order to develop an efficient catalytic system, attention has been paid to the optimization of calcination temperature and reaction temperature in order to achieve complete conversion of methanol for the selective formation of hydrogen. To learn about the interrelationship between the characteristics of the catalyst and catalyst performance in POM, the catalyst characterization included inductively coupled plasma mass spectrometer (ICP-MS), X-ray diffraction (XRD), N_2 adsorption–desorption (BET), temperature-programmed reduction (TPR) and temperature-programmed desorption (TPD) analyses.

2 Experiment

2.1 Preparation of ZnO Support

ZnO support was prepared by precipitation method. The appropriate quantities of $Zn(NO_3)_3 \cdot 6H_2O$ (0.1 mol/L) were dissolved in deionized water with constant stirring. To this solution, polyethylene glycol (PEG-4000) as protection agent was added. Then, $NH_3 \cdot H_2O$ (5 vol.%) was slowly added to it until the pH was adjusted to 9.0. The mixture was refluxed for 3 h at 343 K, filtered and washed with deionized water and ethanol thoroughly. The obtained sample was dried at 343 K overnight and calcined at 673 K for 4 h.

2.2 Catalysts Preparation

The Au–Pd/ZnO catalyst was prepared by an alcohol-reduction method. The appropriate quantities of $HAuCl_4$ (10^{-2} mol/L) and $PdCl_2$ (10^{-2} mol/L) were dissolved in 400 mL mixture solution of ethanol/water (1/1 v/v) containing the polymer poly-*N*-vinyl-2-pyrrolidone (PVP). The mole ratio of PVP and ($HAuCl_4 + PdCl_2$) was 5:1. After adding ZnO support to the solution, the suspension was stirred and refluxed at 363 K for 5 h under N_2. The solvents were removed using rotary evaporator, and the solid was washed several times to eliminate superfluous PVP and Cl^-. The obtained samples were dried in oven at 343 K for 24 h to give a material designated as the catalyst precursor, which was subsequently calcined at 473–1,073 K for 1 h in air. The result of inductively coupled plasma (ICP) indicated that load of the deposit noble metals was 2.0 wt% (Au:Pd = 5:5 wt/wt).

The Au/ZnO and Pd/ZnO catalysts were prepared by the same way as Au–Pd/ZnO catalyst did, loads of Au and Pd in Au/ZnO and Pd/ZnO catalysts were all 2 wt%.

2.3 Catalysts Characterization

The composition of the catalysts was determined by inductively coupled plasma atomic emission spectroscopy (ICP-AES), American PE Corporation's Optima 5300 DV.

Powder X-ray diffractometer (German Bruker-AXS Corporation D8) ($25° \leq 2\theta \leq 50°$; operating at 40 kV and 30 mA) was used at room temperature using Cu Kα radiation combined with the nickel filter. Au size alloy size was calculated by Scherrer formula ($d = k\lambda/B_{1/2}\cos\theta$).

The BET surface area and porous texture were evaluated by N_2 adsorption isotherms obtained at 77 K using an ASAP 2020 (Micrometrics) equipment. Before each measurement, the samples were degassed at 523 K in vacuum (≈ 1 μm Hg) for 2 h. The surface area was calculated with the BET equation.

Temperature-programmed reduction (TPR) was carried out in Chemisorb 2750 instrument over 0.1 g catalyst. The samples were heated from room temperature to 573 K in He (50 mL/min) at a rate of 10 K/min in order to remove possible impurities. After cooling to room temperature in He, a gas mixture consisting of H_2 and Ar (5:95 v/v) was introduced into the system and heated at a rate of 10 K/min for recording the TPR curve.

Temperature-programmed desorption (TPD) was carried out in the in-house apparatus. Before the measurements, the samples were firstly heated from room temperature to 673 K at a rate of 10 K/min and kept at 573 K for 2 h in H_2. After cooling the samples to room temperature in Ar (40 mL/min), CO_2 (or H_2) was pulsed until adsorption was saturated. Then, the samples were heated to 673 K at a rate

of 10 K/min for recording the CO_2-TPD (or H_2-TPD) curve.

2.4 Activity Measurements of the Catalysts

Partial oxidation of methanol was performed in a continuous micro-reactor. The catalyst (100 mg) was reduced in situ first in H_2 flow (30 mL/min) at 573 K for 2 h, and then cooled to the reaction temperature. A gas mixture of CH_3OH (25.0 vol.%), O_2 (7.5 vol.%) and N_2 (balanced) was fed into the reactor and the space velocity was 4,000 mL/h g. The gas composition was analyzed before and after the reaction by a on-line gas chromatograph with thermal conductor detector (TCD). The porapak Q column and 5A molecule sieve column analyzed H_2O, CH_3OH, CO_2, $HCOOCH_3$ and H_2, CO, CH_4, respectively. The catalytic activities of the catalysts were expressed by CH_3OH conversion (%). Hydrogen selectivity and carbon monoxide selectivity was defined as follows:

$$H_2 \text{ selectivity } (\%) = \left(\frac{\text{moles of } H_2 \text{ produced}}{\text{moles of methanol consumed} \times 2}\right) \times 100$$

$$\text{CO selectivity } (\%) = \left(\frac{\text{moles of CO produced}}{\text{moles of methanol consumed}}\right) \times 100.$$

3 Results and Discussion

3.1 Textural Properties of ZnO Support

The morphological character of ZnO support calcined at 673 K was analyzed by nitrogen adsorption–desorption isotherm at 77 K. The result is shown in Fig. 1 and the inset reveals the corresponding pore size distributions. Apparently, the isotherm reveals a clear hysteresis loop when the relative pressure was in a certain range, which illustrates a narrow pore size distribution in the ZnO support. Brunauer–Emmett–Teller (BET) analysis shows that the surface area of ZnO was 36 m^2/g. and from Barrett–Joynor–Halenda (BJH) analysis, its average pore size was 16.9 nm.

3.2 Structural Characterization of the Catalysts

To determine the structure of the support and catalysts in detail, the samples were investigated with XRD. Figure 2 shows the XRD patterns obtained from bulk ZnO, Au/ZnO, Pd/ZnO and Au–Pd/ZnO samples calcined at 673 K. The XRD patterns for ZnO clearly indicate that the peaks observed at $2\theta = 31.6°$, 34.5°, 36.4°, 47.5° and 56.9° were assigned to the diffraction patterns of ZnO(100), (002), (101), (102) and (110) planes, respectively. The diffraction peaks observed at $2\theta = 38.2°$ and 44.4° corresponding to the presence of Au species are clearly visible in the Au/ZnO catalyst. However, only a weak diffraction signal of gold in the profile is observed at $2\theta = 38.2°$ in Au–Pd/ZnO sample. It is noted that two diffraction peaks at $2\theta = 38.9°$ and 44.8° corresponding to Au_xPd_y alloys [18] are observed in the case of Au–Pd/ZnO catalyst, which could be explained by a degree of interaction taking place between some of the Pd and Au species present in Au–Pd/ZnO catalyst. Venezia et al. [18, 19] considered that gold had the tendency to capture palladium in its lattice, forming solid Au_xPd_y alloys enriched in gold species. The existence of the Au_xPd_y alloy was favorable to the improvement of catalytic performance for the Au–Pd/ZnO catalyst. For the Pd/ZnO catalyst, tiny

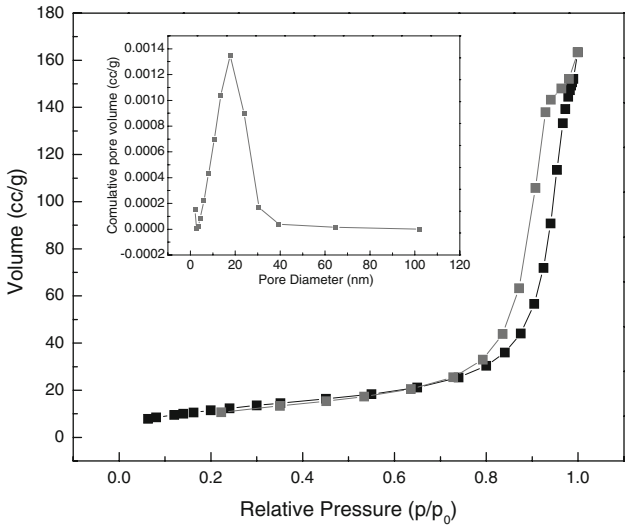

Fig. 1 N_2 adsorption–desorption isotherm of the ZnO support

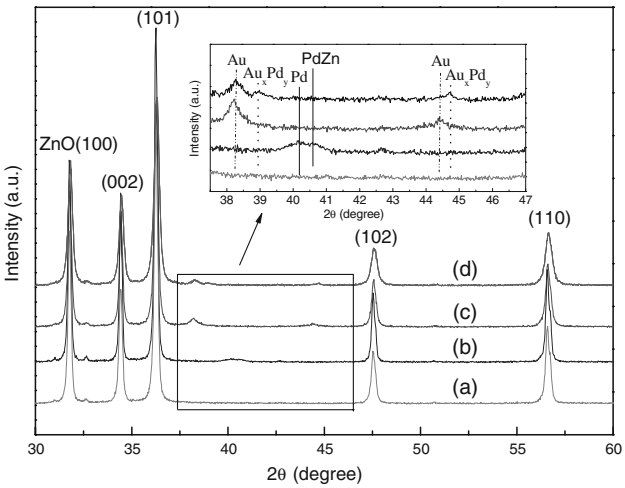

Fig. 2 XRD patterns of the samples: (a) ZnO; (b) Pd/ZnO; (c) Au/ZnO; (d) Au–Pd/ZnO

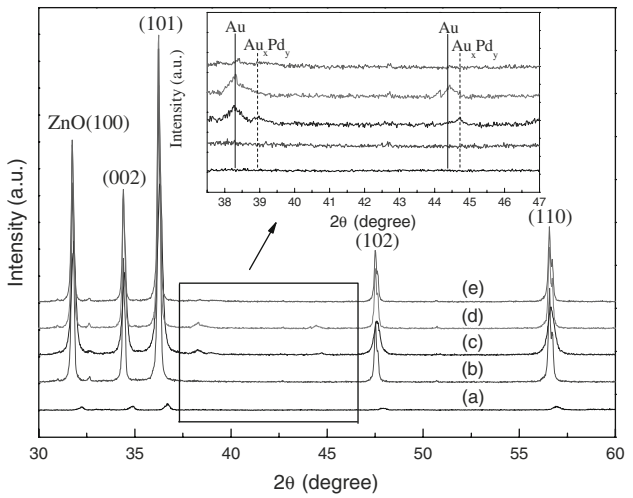

Fig. 3 XRD patterns of Au–Pd/ZnO catalysts calcined at different temperatures: (a) uncalcined, dried at 373 K; (b) 473 K; (c) 673 K; (d) 873 K; (e) 1,073 K

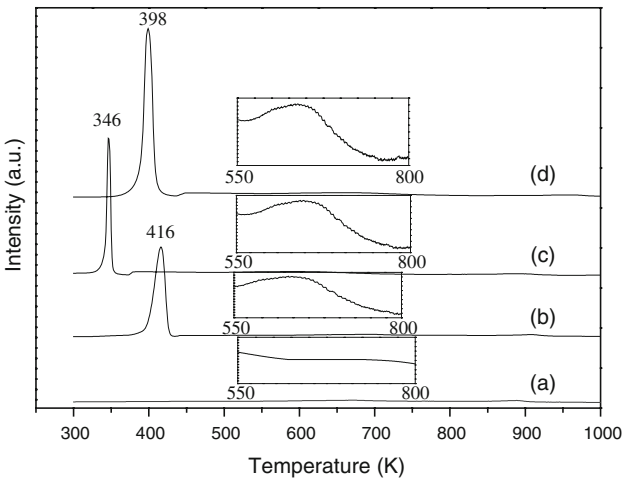

Fig. 4 TPR profiles of the samples calcined at 673 K: (a) ZnO; (b) Au/ZnO; (c) Pd/ZnO; (d) Au–Pd/ZnO

of Pd and PdZn alloys diffraction peak was found from their XRD examinations. The absence of significant diffraction peak for Pd suggested that palladium crystallites were finely dispersed in all of the fresh catalysts. The crystallite size of Au calculated with Scherrer equation in the Au/ZnO and Au–Pd/ZnO catalysts was 8.7 and 6.3 nm, respectively. Obviously, the addition of Pd into Au/ZnO catalyst decreased the particle sizes of gold.

The XRD patterns of Au–Pd/ZnO catalyst before and after calcination at different temperatures are shown in Fig. 3. The peak intensity corresponding to the support (ZnO) was increased with increasing calcination temperature, indicated crystallization increase of the support. The XRD of the uncalcined sample exhibits the presence of hydrozincite ($Zn_5(CO_3)_2(OH)_6$) compounds [20]. Lack of gold peaks at lower calcination temperatures suggests that Au particles are either amorphic, or too small to be detected by XRD. The peak intensity corresponding to gold was increased as increasing calcination temperature, which indicates that the particle size of gold in the catalysts increased as a result of particle sintering, ordering of structure and crystallite growth. However, it is interesting to note that sample calcined at temperatures up to 1,073 K exhibits broad and diffuse peaks, indicating small crystallites and very disordered structure. The reason for the observed disappearance of the specific reflections in the XRD calcined at 1,073 K in the samples may be due to that part Au or Au_xPd_y alloys is sublimated, resulting in the form of the small crystallites or disordered structure.

3.3 TPR Studies

The H_2-TPR can provide information concerning the reducibility of different chemical species presented in the catalyst as well as the degree of interaction between metal–metal and metal–support. The TPR profiles of the bulk ZnO, Pd/ZnO, Au/ZnO and Au–Pd/ZnO catalysts are shown in Fig. 4. A blank TPR experiment using pure ZnO (Fig. 4a) does not exhibit any distinct reduction peak which indicates that pure zinc oxide is difficult to reduce. Whereas we observe high temperature peaks at ca. 650, 690 and 670 K for Au–Pd/ZnO, Pd/ZnO and Au/ZnO catalysts, respectively. The high temperature peak could be attributed to the reduction of ZnO in the presence of noble metals. In the absence of noble metals, temperature in excess of 900 K was required to reduce ZnO, which indicates that Au and Pd exerts a positive influence on the reduction of ZnO. This can be ascribed to hydrogen could be dissociated on nanosized noble metals like Pd or Au, producing atomic hydrogen, which may be favorable to the reduction of the bulk zinc oxide.

As reported [21], Au_2O_3 may be completely transformed into metallic Au when gold catalyst is calcined at 673 K. However, it is clearly seen that a low temperature peak for the Au/ZnO catalyst was observed at 416 K, which may be attributed to the reduction of Au_xO_y and part surface species of ZnO. It could be due to that the strong interaction between Au_2O_3 and ZnO results in its incomplete decomposition to metallic Au under the calcination process. TPR analysis of Pd/ZnO catalyst showed a sharp reduction peaks at 346 K, may be attributed to the reduction of PdO. The TPR profile of Au–Pd/ZnO catalyst is shown in Fig. 4d. The reduction peak due to Au_xO_y, PdO and Au_xPd_yO species centered are overlapped at 398 K. It is clear that the peak is much broader than those seen at low temperature peaks with Au/ZnO and Pd/ZnO catalysts, consistent with two very closely overlapping reduction processes. It is important to note that the reduction peak temperature for oxidic Au and Pd species in bimetallic

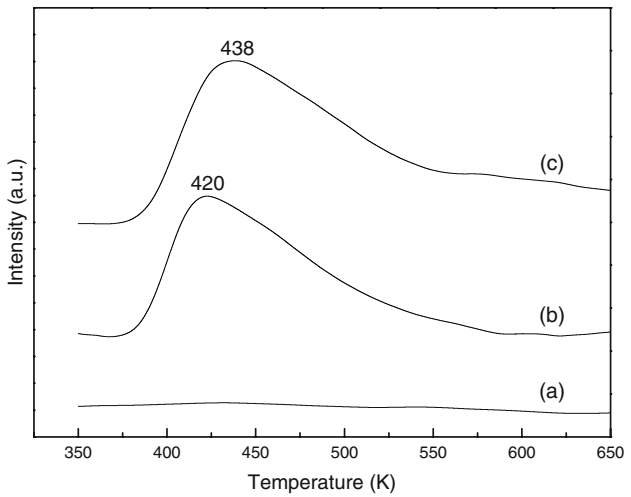

Fig. 5 H_2-TPD profiles of the catalysts: (a) Au/ZnO; (b) Au–Pd/ZnO; (c) Pd/ZnO

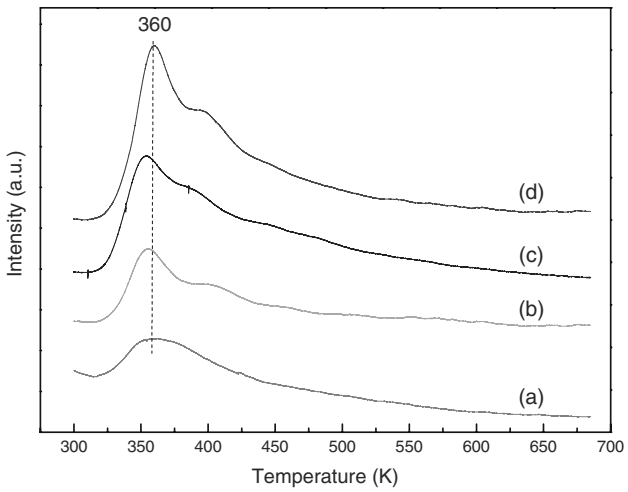

Fig. 6 CO_2 spectra for the samples: (a) ZnO; (b) Au/ZnO; (c) Pd/ZnO; (d) Au–Pd/ZnO

Au–Pd/ZnO catalyst is shifted to higher temperature (398 K) than in monometallic Pd/ZnO, but been lower than Au/ZnO catalyst. This can be ascribed to some sort of interaction between the metals in the bimetallic catalysts. Similar interactions are reported for other bimetallic systems by TPR studies [22, 23]. The moles of H_2 consumed of the low temperature reduction peak for Au/ZnO, Pd/ZnO and Au–Pd/ZnO catalysts is 3.1, 2.9 and 3.7 μmol/g, respectively. A small negative consumption peak was observed for the Pd/ZnO and Au–Pd/ZnO catalysts. This was likely a consequence of H_2 produced during the decomposition of Pd hydrides and Au–Pd hydrides which are known to form at relatively low temperature [24].

3.4 TPD Characterization of the Catalysts

Pulse H_2 chemisorption was used to estimate dispersion degrees of activity sites on the catalysts. The H_2-TPD curves of Pd/ZnO, Au/ZnO and Au–Pd/ZnO catalysts are shown in Fig. 5. Experiment with Au/ZnO catalyst indicated that the support and metal Au did not chemisorbed hydrogen under the conditions employed. As compared with Pd/ZnO catalyst, H_2 desorption temperature of Au–Pd/ZnO catalyst was lower, but the desorption peak areas were almost similar. The higher desorption temperature in the case of Pd/ZnO might be due to the bond energy of Pd–H was stronger than Au_xPd_y–H, and revealed the stronger interaction between the catalyst and support. The lower desorption temperature of Au–Pd/ZnO catalyst makes the reaction product hydrogen is more easily desorption, which is advantageous to chemical reaction. The Pd loading for Pd/ZnO and Au–Pd/ZnO catalysts are 2 and 1 wt%, respectively, however, the chemisorbed hydrogen amounts for these catalysts are almost similar. The quantity of chemisorbed H_2 is inversely proportional to Pd loading, indicating that few palladium exists in metal phase and much more palladium interacts with gold in the Au–Pd/ZnO catalyst [25].

CO_2-TPD is used to characterize the base sites of support and catalyst [26]. These type of sites may have participated in catalyzing POM or reactions of the intermediates. The CO_2-TPD curves were obtained over ZnO, Au/ZnO, Pd/ZnO and Au–Pd/ZnO samples, and there is one CO_2 desorption peak at ca. 360 K, as shown in Fig. 6. The amounts of CO_2 desorption were estimated by integrating areas under the peak temperature up to 425 K. The addition of Au, Pd or Au–Pd to zinc oxide caused an increase in the amount of CO_2 desorption. These results are summarized in Table 1. The increase was much more substantial for the Au–Pd/ZnO catalysts than that of Au/ZnO, Pd/ZnO and ZnO on an areal basis. This may be due to the interaction between the noble metal and the support

Table 1 The amount of desorbed CO_2 form oxide and oxide supported metal catalysts

Catalyst	S_{BET} ($m^2\ g^{-1}$)	Amount of CO_2 desorption		Surface coverage (%)
		mL g^{-1}	molecules cm^{-2}	
ZnO	36	0.65	4.85×10^{13}	4.85
Pd/ZnO	25	0.98	1.05×10^{14}	10.5
Au/ZnO	29	1.1	1.02×10^{14}	10.2
Au–Pd/ZnO	27	1.4	1.39×10^{14}	13.9

The surface coverages were estimated assuming 10^{19} sites m^{-2}

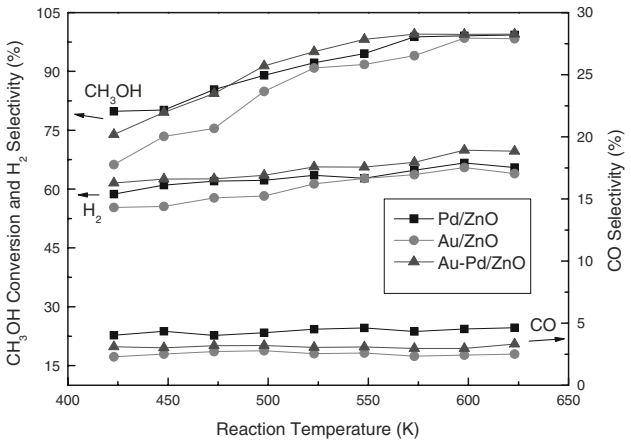

Fig. 7 Activities, hydrogen and carbon monoxide selectivity of the catalysts for POM reaction

and formed Au–O–Zn or Pd–O–Zn. The oxygen atoms with lone-pair electrons on the catalysts surface acts as the electron donor, forming the new alkali centers. It is shown that they play a significant role in increasing the total amounts of desorbed CO_2. The methanol and some intermediates such as formaldehyde were acidic, the more alkali centers were favorable to the POM reaction. The increase in area with no change in desorption peak temperature suggested that the density of sites changed on the addition of noble metal but their qualities were similar.

3.5 Catalytic Activity

Figure 7 shows the effect of reaction temperature on methanol conversion, H_2 selectivity and CO selectivity over Au/ZnO, Pd/ZnO and Au–Pd/ZnO catalysts for POM reaction. The study was undertaken in the temperature range between 423 and 623 K. It can be observed that there is an increase in both methanol conversion and hydrogen selectivity with increasing the reaction temperature. When the reaction temperature is 548 K, these three catalysts showed similar high methanol conversion (91%) and hydrogen selectivity (61.7%). However, Chang et al. [13] studied POM over Au/TiO_2 catalyst: with increasing reaction temperature from 483 to 583 K, the hydrogen selectivity increases from 12 to 35%. The higher hydrogen selectivity of ZnO-supported catalysts was attributed to the behavior of ZnO as a Bronsted base [27], which facilitates the O–H bond cleavage in methanol and forms methoxy species ($CH_3O_{(a)}$), and these species are adsorbed at or near the metal–support perimeter. It was reported that the perimeter interface is the suited place for reaction to take place [28]. As a result, no migration of activated oxygen and the methoxy species are necessary, thereby facilitate the increase of the catalyst activity. The Au–Pd/ZnO bimetallic catalyst exhibited 99.5% methanol conversion and a hydrogen selectivity of 65.6% at 573 K, whereas the monometallic Au/ZnO and Pd/ZnO catalysts had given only a methanol conversion of 91.7 and 94.5%, respectively. Initially, methanol quickly consumes oxygen leading to highly exothermic methanol combustion (MC) reaction to occur and produce water and carbon dioxide ($CH_3OH + 1.5O_2 \rightarrow CO_2 + H_2O$). This is followed by POM reaction (Eq. 3). The high stoichiometric amount of O_2 required for the total oxidation of methanol entails a fast decrease of the O_2 content in the gas. This decrease in the oxidizing potential of the gas phase, together with the excess of energy, implies a progressive removal of surface oxygen species, which favors the dehydrogenation pathway under substoichiometric amounts of surface oxygen. Methanol dehydrogenates to produce methyl formate and hydrogen (Eq. 5) [29].

$$2CH_3OH \leftrightarrow HCOOCH_3 + 2H_2 \quad (5)$$

The selectivity towards methyl formate is decreased with reaction temperature and attains zero at 523 K. This may be due to further decomposition into methanol and CO (Eq. 3) [29].

$$HCOOCH_3 \leftrightarrow CO + CH_3OH \quad (6)$$

When all oxygen available for oxidation has been consumed, the excess of methanol is converted through the endothermic decomposition pathway [MD] (Eq. 7) [29].

$$CH_3OH \rightarrow 2H_2 + CO. \quad (7)$$

The methanol and some intermediates such as formaldehyde were acidic. As we discussed in the Sect. 3.4, the alkali centers of Au–Pd/ZnO catalyst are more than the monometallic Au/ZnO and Pd/ZnO catalysts, the more alkali centers were favorable to adsorption effect of the methanol and intermediates. In addition, the improvement of the performance of the bimetallic catalysts is also due to structural and electronic effects, which arises from a strong metal–metal and metal–support interaction in the catalyst. Therefore synergetic effect between the metal and the support can increase activity of the catalyst for the oxidation reaction. The presence of CO in the reaction product with increasing temperature is due to reaction in Eqs. 6 and 7. It is interesting to note that the Au/ZnO and Au–Pd/ZnO catalysts produced negligible amount of CO. However, carbon monoxide formation appears to be favored by the Pd supported catalyst, significant amount of CO was observed over Pd/ZnO catalyst, being consistent with the results reported in the previous studies on supported palladium catalysts [30]. This is due to smaller Au contained in the catalyst, which consequently enhanced the activity towards direct oxidation of CO in the presence of oxygen.

It is reported that the supported gold catalysts have been proposed as the efficient catalysts for low temperature CO oxidation (Eq. 8) [31].

$$CO + 1/2O_2 \rightarrow CO_2. \quad (8)$$

In addition to that, as water is produced by MC promote WGS, which in turn leads to minimization of CO in the product gas. This may be due to the product formation by the exothermic water gas shift reaction (WGS) (Eq. 9). The supported gold catalyst is also active for the water gas shift reaction [32].

$$CO + H_2O \rightarrow H_2 + CO_2. \quad (9)$$

The catalytic activity of supported Au catalysts strongly depends on the Au particle size, and chemical state of the support [33, 34]. These factors are controlled by varying the calcination temperature. Therefore, it is important to study the effect of calcination temperature on the performance of Au–Pd/ZnO catalysts for POM reaction. Figure 8 shows the effect of calcination temperature on hydrogen selectivity and carbon monoxide selectivity for POM at 523 K. It is clear from the figure that the calcination temperature has a significant influence on the catalytic performance of Au–Pd/ZnO catalyst. The hydrogen selectivity over Au–Pd/ZnO catalysts decreases in the following order: Au–Pd/ZnO (673 K) > Au–Pd/ZnO (873 K) > Au–Pd/ZnO (473 K) > Au–Pd/ZnO (1,073 K) > Au–Pd/ZnO (uncalcined). Thus, the optimum calcination temperature of Au–Pd/ZnO catalyst is 673 K. The lower activity of the uncalcined catalyst is due to the presence of hydrozincite as evidenced from XRD analysis (Fig. 3a). It was reported that the mounts of active gold species available on the catalyst surface could be decreased in the presence of hydrozincite phase [35]. However, the lower activity of the catalyst at higher calcination temperature may be due to the presence of larger Au and Pd particles. High calcination temperature results in sintering of gold and palladium particles and larger particles are formed by coalesces of smaller particles. Highly dispersed Au particles are more active for hydrogen generation [36]. In Fig. 8, the carbon monoxide selectivity over Au–Pd/ZnO catalyst decreases in the following order: Au–Pd/ZnO (uncalcined) > Au–Pd/ZnO (1,073 K) > Au–Pd/ZnO (473 K) > Au–Pd/ZnO (873 K) > Au–Pd/ZnO (673 K). The carbon monoxide selectivity, in particular, is much higher at low calcination temperature. During POM, the carbon monoxide formed by methanol decomposition and/or reverse water gas shift (RWGS) is subsequently oxidized to carbon dioxide. However, this process has been restricted by the presence of hydrozincite [35]. This causes formation of larger amount of carbon monoxide over the uncalcined catalyst. Moreover, for CO oxidation using supported gold catalysts, the particle size of gold plays an important role, smaller gold particles have higher activity. Table 2 summarizes the effect of particle size of gold on the catalytic performance of Au–Pd/ZnO catalysts. The higher carbon monoxide selectivity of the catalyst at higher calcination temperature (873 and 1,073 K) may be due to the presence of slightly larger Au particles as a result of particle sintering. This lead to a conclusion that the Au–Pd/ZnO catalyst calcined at 673 K provides high hydrogen selectivity and low carbon monoxide selectivity.

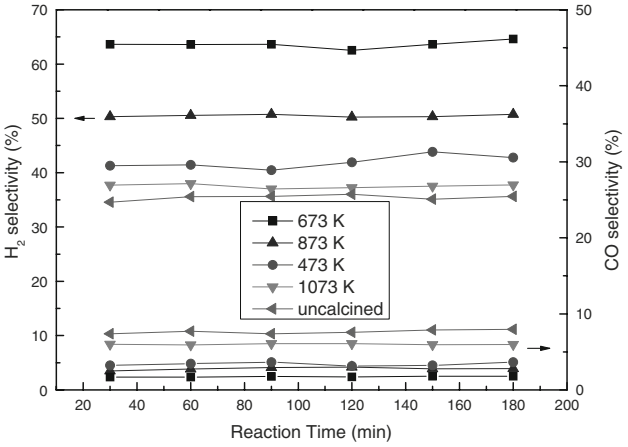

Fig. 8 Effect of calcination temperature on hydrogen selectivity and carbon monoxide selectivity for POM reaction over Au–Pd/ZnO catalysts (reaction temperature 523 K)

Table 2 Catalytic performance of Au–Pd/ZnO catalysts calcined at different temperatures

Calcination temperature (K)	Crystallite size of Au (nm)[a]	H_2 selectivity (%)[b]	CO selectivity (%)[b]
Uncalcined	–	34.6	7.4
473	–	41.3	2.5
673	6.3	63.6	1.7
873	7.2	50.3	3.2
1,073	6.8	37.7	6.0

[a] Calculated from XRD data

[b] Reaction temperature 523 K

The reaction time on methanol conversion and hydrogen selectivity of Au/ZnO, Pd/ZnO and Au–Pd/ZnO catalysts at 523 K shows in Fig. 9. As noted, methanol conversion and hydrogen selectivity decreases with the increases in reaction time. The methanol conversion and hydrogen selectivity remain practically constant for 20 h over the Au–Pd/ZnO catalyst. By contrast, over the Au/ZnO catalyst the methanol conversion and hydrogen selectivity gradually decreased with the increases in reaction time. After 20 h, the methanol conversion and hydrogen selectivity decreased by 24 and 17% of the initial value, respectively. Furthermore, with the increasing the reaction time, a little

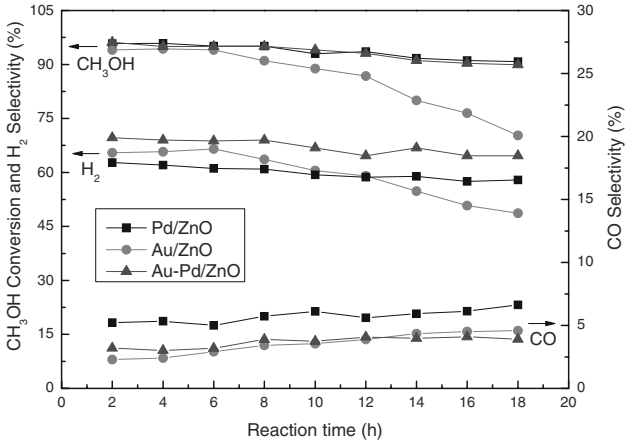

Fig. 9 Stabilities of the catalysts for POM reaction (reaction temperature 523 K)

increase in CO selectivity could be observed. The deactivation of Au/ZnO catalyst is ascribed to growth of gold particle during the reaction. It is reported that highly dispersed small Au particles are more active for CO oxidation, while larger Au particles are more active for hydrogen oxidation [36]. It is important to note that the Au–Pd/ZnO bimetallic catalyst shows good stability during the catalytic runs as well as high activity and H_2 selectivity for the POM reaction. However, the deactivation for the industrial catalyst $CuO/ZnO/Al_2O_3$ was quickly [37].

4 Conclusions

The present result reveals that Au–Pd/ZnO catalyst is more active to produce hydrogen by POM reaction compared to Au/ZnO and Pd/ZnO catalysts. The enhanced activity and stability of the Au–Pd/ZnO bimetallic catalyst is attributed in terms of the synergetic effect of gold and palladium species, higher dispersion and smaller particles of gold. Studies on the catalytic behavior of the Au–Pd/ZnO catalyst at different calcination temperatures demonstrate that chemical state of the support and particle size of Au and Pd plays an important role. The optimum calcination temperature for hydrogen selectivity is 673 K. The effect of reaction temperature on the performance of the Au–Pd/ZnO catalysts was studied in the temperature range of 423–623 K. Both methanol conversion and hydrogen selectivity are increasing with increasing reaction temperature. Almost complete conversion of methanol is observed above 598 K. The hydrogen selectivity of 65.6% with very low CO selectivity of 3.1% is observed at 573 K. The present study suggests that the Au–Pd/ZnO catalyst is a relative well catalyst for POM reaction.

References

1. Katikaneni S, Gaffney AM, Song C, Apple AJ, Foulkes FR (2002) Catal Today 1–2:77
2. Cheng WH (1995) Appl Catal A 130:13
3. Xi J, Wang Z, Lu G (2002) Appl Catal A 77:225
4. Ito S, Suwa Y, Kondo S, Tameoka S, Tomishige K, Kumimori K (2000) Catal Commun 1:499
5. Shishido T, Yamamoto Y, Morioka H, Takaki K, Takehira K (2004) Appl Catal A 263:249
6. Chen GW, Li SL, Li HQ, Jiao FJ, Yuan Q (2007) Catal Today 97–102:125
7. Murcia-Mascaro′s S, Navarro RM, Go′mez-sainero L, Costantino U, Nocchetti M, Fierro JLG (2001) J Catal 198:338
8. Cubeiro ML, Fierro JLG (1998) Appl Catal A 168:307
9. Agrell J, Birgersson H, Boutonnet M, Melia′n-Cabrera I, Navarro RM, Fierro JLG (2003) J Catal 219:389
10. Mo LY, Zheng XM, Yeh CT (2004) Chem Commun 1426–1427
11. Yang HC, Chang FW, Selva Roselin L (2007) J Mol Catal A 184–190:276
12. Huang TJ, Wang SW (1986) Appl Catal 24:287
13. Chang FW, Yu HY, Selva Roselin L, Yang HC (2005) Appl Catal A 290:138
14. Chang FW, Yu HY, Selva Roselin L, Yang HC, Ou TC (2006) Appl Catal A 302:157
15. Haruta M, Yamada N, Kobayashi T, Iijima S (1989) J Catal 115:301
16. Stytsenko VD (1995) Appl Catal A 1:126
17. Lu P, Teranishi T, Asakura K, Miyake M, Toshima N (1999) J Phys Chem B 103:9673
18. Venezia AM, Parola VL, Nicol V, Deganello G (2002) J Catal 212:56
19. Venezia AM, Parola VL, Deganello G, Pawelec B (2003) J Catal 215:317
20. Aiejo L, Lago R, Pena MA, Fierro JLG (1997) Appl Catal A 162:281
21. Wang GY, Jia MJ, Yu JF, Li XM, Zhang WX, Jiang DZ, Wu TH (2000) Chin J Catal 569:21
22. Zhiqinga Z, Zihonga L, Bina L, Shizhuo G (2006) Appl Catal A 302:208
23. Cheekatamarla PK, Lane AM (2005) Int J Hydrogen Energy 30:1277
24. Iwasa N, Mayanagi T, Nomura W, Arai M, Takezawa N (2003) Appl Catal A 248:153
25. Bonarowska M, Pielaszek J, Semikolenov VA, Karpinski Z (2002) J Catal 209:528
26. Hattori H (2004) J Jpn Petrol Inst 47:67
27. Idem RO, Bakhshi NN (1955) Ind Eng Chem Res 34:1548
28. Haruta M, Tsubota S, Kobayashi T, Kageyma H, Genet MJ, Delmon B (1993) J Catal 144:175
29. Chang FW, Lai SC, Roselin LS (2008) J Mol Catal A 282:129
30. Cubeiro ML, Fierro JLG (1998) J Catal 179:150
31. Haruta M (1997) Catal Today 36:153
32. Fu Q, Deng Wl, Saltsburbg H, Maria FS (2005) Appl Catal B 56:57
33. Grunwaldt JD, Maciejewski M, Becker OS, Fabrizioli P, Baiker A (1999) J Catal 186:458
34. Horva′th D, Toth L, Guczi L (2000) Catal Lett 67:117
35. Wang GY, Zhang WX, Lian HL, Jiang DZ, Wu TH (2003) Appl Catal A 1:239
36. Choudhary TV, Sivadinarayana C, Chususei CC, Datye AK, Fackler JP, Goodman DW (2002) J Catal 207:247
37. Grisel RJH, Weststrate CJ, Goossens A, Craje MWJ, Vanderkraan AM, Enieuwenhuys B (2002) Catal Today 72:123